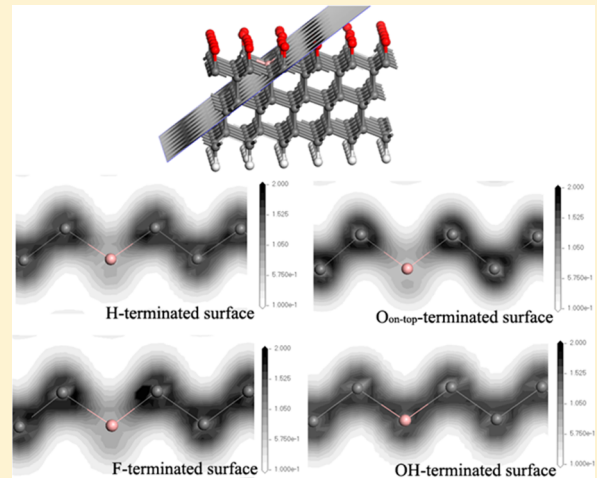


Theoretical Study of the Energetic Stability and Geometry of Terminated and B-Doped Diamond (111) Surfaces

Shuainan Zhao* and Karin Larsson

Department of Chemistry Ångström Laboratory, Uppsala University, Uppsala, Sweden

ABSTRACT: The effect of B doping on the surface (111) reactivity has, in the present study, been investigated for various surface terminations, H, OH, O_{on-top}, and F. This type of surface modification has experimentally been proven to be extremely important for, for example, applications based on surface electrochemistry. Density functional theory (DFT) has here been used to study both the local and more global effects of substitutionally positioned B atoms in the upper part of the diamond (111) surface. For this purpose, adsorption energies for the various terminating species have been calculated, and the observed results have been carefully analyzed in order to gain a deeper knowledge about the atomic-level cause of the observed effects. As a result, the B dopant shows a clear, but local, effect for all terminating species investigated. In addition, it is only the radical O-terminating species that show a special and high reactivity on the diamond surface. The other terminating species show a much lower reactivity, which in addition are very similar.



1. INTRODUCTION

The diamond material possesses very attractive properties, such as high transparency and high thermal conductivity at room temperature. However, diamond material with its intrinsic band gap of 5.5 eV and low electronic conductivity will limit applications based on electronic devices. When introducing boron into diamond during thin film deposition, the B dopant will increase the electronic conductivity, which gives a material with extraordinary electrochemical properties.¹ Boron-doped diamond is a semiconducting material with very promising properties like (i) a wider potential window in aqueous solution (approximately -1.35 to +2.3 V versus the normal hydrogen electrode),² (ii) low background current, and (iii) corrosion stability in aggressive environments. Thus, boron-doped diamond surfaces are nowadays used for a variety of electronic applications.^{3–5}

During the process of diamond synthesis, the resulting chemical properties will mainly depend on the number of surface radical C sites (i.e., dangling bonds) and the adsorbed (especially chemisorbed) species. The sp³ hybridization of the carbon atoms, leading to strong and directional σ bonds, is decisive for the extreme physical properties of the material. The existence of dangling bonds on the surface makes monocrystalline diamond quite reactive. Moreover, the chemisorbed adsorbates may prevent the diamond surface from being graphitized (go from sp³ toward sp² hybridization). This is partially why a supersaturation of hydrogen is used in the reaction chamber during growth of diamond.⁶ In addition, the chemisorbed species will have the ability to influence the chemical and electronic properties of diamond,^{7,8} such as field

emission characteristics,⁹ surface wettability, and electrochemical properties of the diamond surface.¹⁰

Surface termination is the general notation when a species (e.g., H, O, F) is used with the purpose to uphold the cubic structure or to change the surface properties. The phenomena of diamond surface termination have experimentally been observed to significantly influence the broad-band infrared reflectivity and conductivity.¹¹ Hydrogen-terminated diamond surfaces have been found to be hydrophobic¹² and to show electron transfer across the interface.¹³ On the other hand, oxygen-terminated diamond surfaces generally show hydrophilic properties¹⁴ and exhibit fast heterogeneous electron transfer while maintaining low background signals with the wide extended solvent window properties.¹⁵ In addition, OH-terminated surfaces can be formed during etching in a mixture of oxygen and water vapor.¹⁴ This type of surface termination is often desired; different chemical routes can be used to link functional groups to these OH adsorbates, for further use in, for example, electroanalytical applications.¹⁶ Fluorine termination will, compared to H termination, result in even more strongly hydrophobic diamond surfaces. These surfaces will also exhibit exceptional electrochemical properties and low capacity currents.¹⁷ All of these interesting properties of terminated diamond surfaces make it clear that surface termination is very important for especially those applications in which diamond can function as an electrode material. The relative reactivity for

Received: September 17, 2013

Revised: December 19, 2013

Published: December 30, 2013

the various diamond surface planes, terminated with either H, O, OH, or F, are therefore very important to study from an atomic-level point of view.

Theoretical modeling has, during the last decades, been proven to become highly valuable in the explanation and prediction of experimental results. The simulation of surface reactivity can aid important information about thin film growth mechanisms, as well as about surface reconstruction, modification, and functionalization. The low-index (111) plane is one of the most frequently obtained surface planes in CVD-grown crystalline diamond. The origin of surface reactivity for nonterminated diamond surfaces,^{18,19} as well as the energetic stability of the terminated (111) surfaces,²⁰ was earlier studied by the present group using density functional theory (DFT). What is missing today is the corresponding study for also boron-doped diamond (111) surfaces. The purpose of the present study has therefore been to theoretically investigate the energetic stability and surface reactivity for B-doped and variously terminated diamond (111) surfaces using DFT under periodic boundary conditions. The models used in the calculations include H, OH, F, O_{on-top}, and O_{bridge} terminations, as well as nonterminated diamond surfaces. Both B-doped and nondoped diamond (111) surfaces were used in the study, with the main goal to make a structural and energetic investigation of the combined effect of B doping and termination type. Only 100% surface coverage (for all types of terminating species) was considered in the present study.

2. METHODOLOGY

All calculations in the present study have been performed using DFT^{21,22} under periodic boundary conditions. More specifically, an ultrasoft pseudopotential²³ plane wave approach was used, using the Perdew–Wang (PW91) generalized gradient approximation (GGA)²⁴ for the exchange–correlation functional. The GGA method usually gives a better overall description of the electronic subsystem, compared to the more simple LDA (local density approximation) corrections. The reason is that LDA, which is based on the known exchange–correlation energy of a uniform electron gas, is inclined to overbind atoms and to overestimate the cohesive energy in the system under study. On the contrary, GGA takes into account the gradient of the electron density, which gives a much better energy evaluation.¹⁹ All of the calculations in the present work were carried out using the Cambridge Sequential Total Energy Package (CASTEP) program from Accelrys, Inc.²⁵

All individual models consisted of more than 200 atoms in the supercell, and thus, the value of the energy cutoff for the plane wave basis sets was comparably small and set to 380.00 eV. Due to the large size of the model, this numerical value should be adequate for the present study. In addition, the Monkhorst–Pack scheme²⁶ was used for the *k*-point sampling of the Brillouin zone, which generated a uniform mesh of *k* points in reciprocal space. The 1 × 1 × 1 *k*-point, as well as the cutoff frequency of 380 eV, was earlier found to be adequate to use for the present type of system.²⁷ Due to the presence of unpaired electrons in the systems, all of the calculations were based on spin-polarized GGA. The atomic charges and bond electron populations were estimated by using the methods of Mulliken analysis, which is performed using a projection of the plane wave states onto the localized basis by a technique described by Segall et al.²⁸ As will be more deeply described in section 3.C, the calculated atomic charges, electron density (ρ),

Fukui function (FF), and information about bond electron populations (i.e., electron densities) were important tools in the interpretation of the underlying causes to the effects of (i) terminating species and (ii) B doping.

The FFs of the surface area generally have been used in visualizing the surface reactivity. Parr and Yang^{29,30} improved the frontier orbital theory introduced by Fukui,^{31,32} whereby it became possible to calculate the so-called FFs

$$f(r) = \left(\frac{\delta\rho(r)}{\delta N} \right)_V \quad (1)$$

where N is the total number of electrons in the system and $\rho(r)$ is the electron density at a certain position and at a fixed external potential, V . There are three FFs defined as f^0 , f^+ , and f^- , which correspond to a surface reactivity toward radical, electrophilic, and nucleophilic attack, respectively. Previous work has shown that this f^0 function can be very useful in studying the surface reactivity of diamond.^{19,20} The program Dmol³ from Accelrys Inc. was in the present study used for these Fukui functional calculations.^{33,34}

The atomic charges were also carefully estimated to give information about the degree of ionic bond strengths, while the bond populations contribute with covalent bond strength information. All of these factors are furthermore helpful in the understanding of surface restructuring.

The averaged adsorption energies associated with the chemisorption of the terminating species H, OH, F, O_{on-top}, and O_{bridge}, were calculated using eq 2

$$E_{\text{ads,avg}} = \frac{1}{n} [E_{\text{surface}} - E_{\text{bare-sur}} - nE_n] \quad (2)$$

where E_{surface} is the total energy of the 100% terminated surface, $E_{\text{bare-sur}}$ is the total energy of a clean (i.e., nonterminated) surface, n is the number of a specific terminating species within the supercell, and E_n is the total energy of the adsorbing gas-phase species (i.e., O, OH, H, and F). This averaged value will give information about the more global effect on the B dopant (i.e., on the whole surface within the supercell). In addition, the adsorption energy $E_{\text{ads,last}}$ of an individual terminating species in the closest vicinity to the B dopant was also calculated in order to receive information about the more local effect of the B dopant

$$E_{\text{ads,last}} = E_{\text{surface}} - E_{\text{radical}} - E_n \quad (3)$$

where E_{surface} is the total energy of the 100% terminated surface, E_{radical} is the total energy of the otherwise terminated surface with a radical bare site in the supercell, and E_n is the total energy of the adsorbing gas-phase species (i.e., O, OH, H, and F).

As a result of chemical vapor-phase deposition (CVD) of diamond thin films, there are usually different low Miller index planes that will dominate on the surface; (111) and the 2 × 1-reconstructed (100) surfaces are the most frequently observed ones. The (111) surface has in the present investigation been chosen for studying diamond surface properties and reactivity tendencies (see Figure 1). A six carbon layer thick diamond slab, with the cell dimensions of 5 × 5, was used for all surface models, with the purpose to properly simulate the reconstruction and relaxation of the various types of diamond planes. This model size was proven by earlier investigations to be adequate to use for the present type of study.³⁵ The diamond surfaces were terminated to 100% with any of the following species: (a)

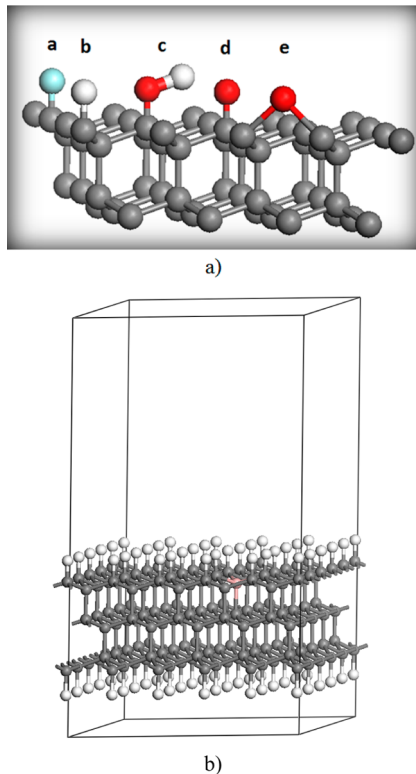


Figure 1. (a) Five different types of surface-terminating species, chemisorbed onto a diamond (111) surface: (a) F, (b) H, (c) OH, (d) O_{on-top}, and (e) O_{bridge}. (b) Model of the H-terminated diamond (111) surface. The H, B, and C atoms are shown in white, pink, and gray.

F, (b) H, (c) OH, (d) O in the ketone position (O_{on-top}), and (e) O in ether positions (O_{bridge}). In addition, one boron atom was substitutionally positioned within the second C layer. This position will render an appreciable effect on the diamond growth rate and especially on the rate-determining H-abstraction step. The energy barrier for this abstraction step was found to be reduced to zero for the diamond surfaces (111), (100)-2×1, and (110). To suppress the artificial charge transfer between the two polar ends of the slabs, the dangling bonds on the lower surfaces of the slabs were saturated with H atoms, and a large vacuum distance between the slabs was used (>7 Å).^{19,20} The reason to saturate the lower C atoms with hydrogen atoms was also to saturate the dangling bonds and to simulate the continuation of bulk diamond. These H atoms were therefore, together with the lowest C layer, kept fixed during the geometry optimization process. The rest of the atoms in the model systems were allowed to freely relax using the BFGS algorithm (Broyden–Fletcher–Goldfarb–Shanno).³⁵

3. RESULTS AND DISCUSSION

A. Adsorption Energy As a Measure of Surface Reactivity. The surface reactivity of a certain material is generally determined by the number of Fermi level electrons and can be estimated by different means. One way is to calculate the chemisorption energy for some specific model adsorbates. Within the present study, the chemisorption of H, F, and O onto B-doped diamond (111) surfaces was studied in order to elucidate the reactivity toward these terminating species. Each of them is most frequently used in the growth process, during surface functionalization, and for surface

modifications (as presented in the Introduction). It is therefore of largest interest to investigate in more detail the effect of each of these termination scenarios on the surface reactivity of the diamond (111) planes, being one of the most common low-index planes in micro- and nanocrystalline diamond thin films. The averaged chemisorption energy $E_{\text{ads},\text{avg}}$ was used for studying the more global effect of B doping, while the local effect was obtained by calculating the adsorption energy $E_{\text{ads},\text{last}}$ for one of the terminating species (on an otherwise 100% terminated surface) that is being bonded to the surface on a position closest to the B atom in the lattice. There are in fact three adsorbates that have this neighboring position, which all link to the B atom via only one C atom. These adsorbates are from here on called adjacent adsorbates.

As can be seen in Table 1, the calculated averaged chemisorption energies showed that there is no significant

Table 1. Averaged Adsorption Energies (eV per adsorbate) and Adsorption Energies (eV) for an Otherwise 100% Terminated Surface for Both B-Doped and Nondoped Diamond (111) Surfaces

| surfaces | species | H | OH | O on top | F |
|----------|-------------|-------|-------|----------|-------|
| nondoped | average | -4.34 | -3.86 | -5.06 | -4.58 |
| | last specie | -4.38 | -3.43 | -4.90 | -4.27 |
| B-doped | average | -4.28 | -3.82 | -5.04 | -4.52 |
| | last specie | -3.44 | -3.33 | -4.28 | -3.34 |

global effect of B doping. The differences in averaged chemisorption energy, $\Delta E_{\text{ads},\text{avg}}$, for the B- and nondoped diamond surfaces are very small, $0.02 < \Delta E_{\text{ads},\text{avg}} < 0.06$ eV. In fact, these numerical differences are almost negligible and within the error of limits for the theoretical method used. However, when comparing the averaged adsorption energy, $E_{\text{ads},\text{avg}}$, with the adsorption energy for only one adsorbate, $E_{\text{ads},\text{last}}$ (onto an otherwise 100% terminated surface), it is obvious that the local effect of B doping is quite substantial. The values of $E_{\text{ads},\text{last}}$ are for all adsorbate types less than the averaged $E_{\text{ads},\text{avg}}$. In addition, the lower values for $E_{\text{ads},\text{last}}$ relative to $E_{\text{ads},\text{avg}}$ for the nondoping scenario reflect the existence of steric repulsions among the adsorbates for 100% surface termination.

Even though there is no evidence for a global effect by the dopants, there is an apparent local effect that affects the adjacent adsorbates. The difference in adsorption energy for the B- and nondoped surfaces, $\Delta E_{\text{ads},\text{last}}$, is substantial and cannot be neglected ($0.10 < \Delta E_{\text{ads},\text{last}} < 0.94$ eV). Thus, it is thereby confirmed that the B dopant will induce a weakening effect on the bonds between the three adjacent adsorbates and their binding surface C atoms.

The averaged adsorption energies clearly show that it is the O_{on-top} adsorbate that will be most efficient (of the four adsorbate types) in stabilizing the diamond (111) surfaces, with almost identical values for the nondoped and B-doped scenarios (-5.06 versus -5.04 eV). Unfortunately, it was not possible to achieve a stable 100% surface coverage with O in O_{bridge} formation. The underlying reason is most probably the low number of unpaired electrons per surface C site. The diamond (111) surface has only one unpaired electron per surface C atom, which forces the terminating O atom to bind to two surface C atoms and with a maximum surface coverage of 50%. An earlier theoretical investigation by D. Petrini and K. Larsson also showed that an O_{bridge} surface coverage larger than 25% will render highly unstable diamond (111) surfaces.²⁰

Hence, when initially positioning the O in O_{bridge} formations at 100% coverage, the O–O bridge bonds were in the present study observed to break during the geometry optimization and to instead form O_{on-top} formations (at 100% coverage). It is thereby possible to conclude that a very high concentration of O atoms at the surface may force the surface composition into O_{on-top} positions. It must be emphasized that this observation was made as a result of 0 K calculations, and hence, there is no energy barrier involved in this structural reorganization (from initial bridge to on-top O positions). As presented above, the effect of the B dopant is more obvious when calculating the adsorption energy for an adjacent adsorbate; $E_{\text{ads},\text{last}} = -4.28 \text{ eV}$ for a B-doped O-terminated surface, which is less exothermic compared to $E_{\text{ads},\text{last}} = -4.90 \text{ eV}$ for a nondoped surface.

A 100% termination with OH species resulted in an averaged adsorption energy (-3.86 eV for nondoped versus -3.82 eV for B-doped) that is less favorable than that for O adsorption and is also the least favorable termination type within the present study. The underlying reasons to this result are most probably the degree of steric hindrances induced by neighboring OH adsorbates. There is in fact two competing interadsorbate interactions, (i) hydrogen bonding and (ii) induced steric repulsions. The former one will stabilize the surface system, and the latter will destabilize and thereby weaken the surface–adsorbate bonds. The steric effect can be further visualized by studying the values of adsorption energies for the nondoped situation, $E_{\text{ads},\text{avg}} = -3.86 \text{ eV}$ and $E_{\text{ads},\text{last}} = -3.43 \text{ eV}$. The adsorption of the last OH species, on an otherwise completely OH-terminated diamond surface, showed the largest difference in energy (compared to an average value for a 100% termination), 0.43 eV . The combined effect by the adsorbates can be further observed by studying the values of adsorption energies for the adjacent adsorbates ($E_{\text{ads},\text{last}}$), -3.33 (B doping) versus $-3.43 \text{ (nondoping) eV}$. These two values represent the smallest difference in adsorption energy in the present study (0.1 eV) when comparing B- and nondoped surfaces for all different termination types. The most plausible explanation to this observation is that the effect of the B dopant will be somewhat “concealed” by the influence of the steric repulsions among the OH adsorbates.

The F adsorbate showed the second most efficient tendency to form stable diamond (111) surfaces, with averaged adsorption energies of $-4.58 \text{ (nondoped surface)}$ and -4.52 eV (B-doped surface). These numerical values were very similar to the results obtained for the H-terminated surfaces, $-4.34 \text{ (nondoped surface)}$ and -4.28 eV (B-doped surface). In addition, the numerical values for H and OH termination are also rather similar and are both on the low-energy edge of the adsorption energy trend for these adsorbate types, $-3.86 \text{ (nondoped OH-terminated surface)}$ and -3.82 eV (B-doped OH-terminated surface). These results are strongly supported by the calculations of adsorption energies for the adjacent terminating species: H-terminated surface ($-4.38 \text{ (nondoped surface)}$) and -3.44 eV (B-doped surface)), F-terminated surface ($-4.27 \text{ (nondoped surface)}$ and -3.34 eV (B-doped surface)), and OH-terminated surface (-3.43 eV (nondoped surface) and -3.33 eV (B-doped surface)). These results show that the diamond (111) reactivity toward H versus F is very similar and only somewhat more pronounced compared to that for OH. The underlying cause for the much higher reactivity toward O will be analyzed and discussed in section 3.C. Furthermore, the present study has revealed a larger destabilizing effect by the B dopant on the adjacent H and F

adsorbates, compared to that on the O and OH adsorbates. The reason for this induced bond-weakening effect by B will be further discussed in the text below.

B. Adsorption-Induced Surface Geometrical Restructuring. In nondoped diamond, all C–C bonds are electron pair single bonds because the C atom has four valence electrons and is bonded to four other C atoms (i.e., sp³ hybridized). When one boron atom will substitutionally replace one carbon atom within the second C layer, an element has been introduced into the diamond lattice with one less valence electron. Hence, the four bonds between the B atom and its four neighboring C atoms must be deficient by a total of one electron. A B dopant in this position will result in a zero energy barrier for the H abstraction reaction from the surface and has therefore been chosen as the preferable position in the present study. The underlying cause for this effect is the electron redistribution within the surface region due to introduction of the three-valence B element into the structure.

As the result of the geometry optimization in the present study, all B–C bonds were elongated to different extents for the B-doped and surface-terminated diamond (111) surfaces (as compared with the C–C bonds in diamond; 1.54 \AA). This result agrees with a recently experimental work performed by Lu et al., who showed that local bond elongation will take place in boron-doped diamond.³⁶ This is an indication of bond weakening and does fit very well with the deficiency of one electron in the vicinity of B. However, the situation was completely different for the nonterminated B-doped diamond surface. The bond length between the B atom and the three binding surface C atoms in the first C layer decreased, while the bond length between the B atom and third-layer C atom increased. As a result of these bond length changes, the B atom moved up toward the layer of surface C atoms (see Figure 2).

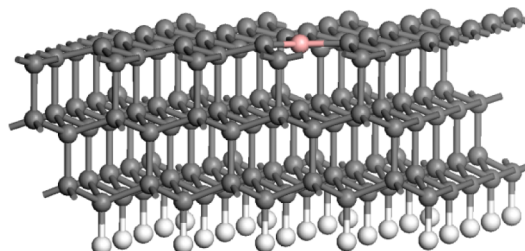


Figure 2. The model of a geometry-optimized B-doped diamond (111) surface without any surface termination.

The longest B–C distance is 1.946 \AA , which is quite longer than the other three B–C bonding lengths (1.510 – 1.512 \AA). These results give evidence of the preferred valence electron configuration by B (i.e., by forming only three covalent bonds to neighboring C atoms). Moreover, the three binding surface C atoms showed very small negative atomic charges (-0.09 to -0.12), which is an indication of almost perfectly covalent bonds with minor ionic contributions. In addition, the bonds between the three surface C atoms and the B dopant were found to display larger electron bond populations (0.92 – 0.94) compared to the bond between the third-layer C atom and the B dopant (0.39 for bond population), which again supports the observation of a weakened covalent bond formation to the lower C carbon.

As can be seen in Table 2, the bond lengths between the adjacent adsorbates and the surface carbon atoms that are binding to the B dopant ($r_{\text{A}-\text{C}}$) have also become influenced by

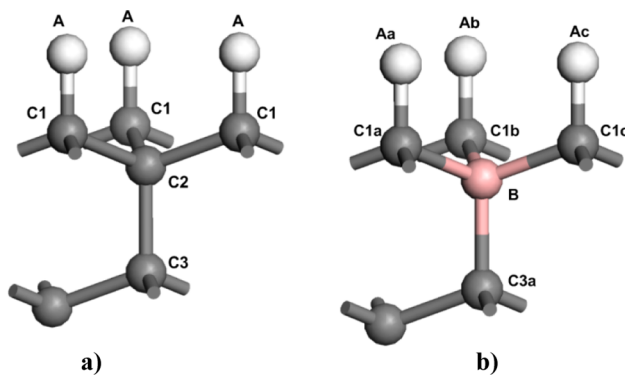


Figure 3. Atomic structure of the (a) nondoped and (b) B-doped diamond (111) surface, visualizing the upper layer carbon, boron, and adsorbate atom positions. For the nondoped diamond model, the abbreviations are as follows: A: adsorbate; C1: carbon atoms in the first layer; C2: carbon atom in the second layer; C3: carbon atom in the third layer. For the B-doped diamond model, the abbreviations are as follows: Aa, Ab, Ac: adjacent adsorbates; C1a, C1b, C1c: carbon atoms in the first layer (binding to the doping boron atom); B: boron atom substitutionally positioned in the second C layer; C3a: carbon atom in the third layer (binding to the doping boron atom).

the B doping. There is an observed bond lengthening for the adsorbates H, F, and OH, while the O adsorbate gives a shortened length. However, the effect of B doping on the bond lengthening is not so pronounced; it is at most 0.02 Å. The largest change in bond length is observed for the OH-terminated surface (0.02 Å). The underlying reason for this observation is most probably the induced steric hindrances between the OH adsorbates, which also may explain the rather low adsorption energy for this type of adsorbate (as discussed in section 3.A).

For adsorbate–C_{surface} bonds farther away from the B doping element, there was, for all terminating species investigated, no observable influence by B on the bond lengths. This was also the situation for all C–C bonds at a distance larger than 3 Å from B. Hence, it is thereby possible to conclude that the combined effect by the boron doping and type of adsorbate will only affect the upper surface region most adjacent to the B dopant.

C. Analysis on the Electronic Level. The boron element does only have three valence electrons, while the carbon element has four. As stated above, the B dopant will thereby introduce a deficiency of electrons within the system. Furthermore, the electronegativities of the C and B atoms are 2.55 and 2.04, respectively.³⁷ Thus, a polarization of electron density within the B–C bond, with the preference for electrons

in the vicinity of the C atom, is highly expected. In the present systems, however, not all of the C atoms within the B–C bonds showed negative charges. The reason for this observation is most probably the effect of the adjacent adsorbates binding to these C atoms. Despite this circumstance, the B atoms were still observed to donate electrons to the binding C atoms and thereby to show a more positive charge compared to the C atom.

1. Atomic Charge Calculations and Mulliken Bond Population Analysis. The total electron density maps have been calculated for the various systems in the present investigation, diamond (111) surfaces that are terminated with either H, OH, O_{on-top}, or F species (see Figure 4). The purpose with these plots is to provide an overview of electron redistribution when substituting a B atom into the diamond lattice. In addition, Table 3 shows the Mulliken bond population analysis for the B–C bonds within these systems. The molecule H₆C₂BC₃H₉ (see Figure 5) has been used as a reference compound for B–C bond comparison. The bond population of B–C in H₆C₂BC₃H₉ is 0.87, with a corresponding bond length of 1.596 Å. It must be stressed that this bond length is somewhat prolonged due to the steric repulsions between the three-dimensional CH₃ groups that are residing on the B and C atoms. Thus, it is highly expected that a more realistic bond population of a B–C bond (i.e., without the influence of steric hindrance) should be even larger than the value of 0.87. As visualized in Figure 4, there is a weakening within the B–C_{surface} bonds in the diamond surfaces for all termination types. The bond population analyses confirm this observation. For the O_{on-top} termination, the electronic bond population between the B atom and each of the three surface C atoms is within the interval 0.65–0.70, which is on the lower range when compared to the other termination types (0.79–0.85). The surfaces with H, OH, or F terminations resulted in bond populations of 0.77–0.83 (H), 0.73–0.82 (F), and 0.80–0.84 (OH), the latter being the largest values for all four termination scenarios. It must be stressed that all of these values are smaller than that for an ordinary covalent single B–C bond (0.87 as in H₆C₂BC₃H₉). This reflects the fact that there are fewer electrons involved in the formation of bonds between the B dopant and the surrounding C atoms within B-doped diamond, which leads to bond weakening because the binding orbitals will not be fully occupied. This bond weakening has been identified with bond lengthening, as discussed in section 3.B.

In addition, this assumed bond weakening effect is further supported by the total electron density maps, which all demonstrate a lower electron density (i.e., brighter color)

Table 2. Bond Lengths (in Å) for Nonterminated or Completely H-, OH-, O-, or F-Terminated B-Doped versus Nondoped Diamond (111) Surfaces^a

| | B-doped surfaces | | | | | | | nondoped surfaces | | |
|---------------------|------------------|--------|--------|-------|-------|-------|-------|-------------------|-------|-------|
| | Aa–C1a | Ab–C1b | Ac–C1c | B–C1a | B–C1b | B–C1c | B–C3a | A–C1 | C1–C2 | C2–C3 |
| clean | | | | 1.512 | 1.510 | 1.510 | 1.946 | | 1.497 | 1.634 |
| H | 1.109 | 1.109 | 1.107 | 1.583 | 1.596 | 1.574 | 1.624 | 1.108 | 1.531 | 1.552 |
| OH | 1.439 | 1.451 | 1.460 | 1.583 | 1.593 | 1.563 | 1.583 | 1.429 | 1.536 | 1.548 |
| O _{on-top} | 1.315 | 1.305 | 1.302 | 1.630 | 1.652 | 1.654 | 1.578 | 1.321 | 1.569 | 1.525 |
| F | 1.396 | 1.389 | 1.399 | 1.572 | 1.604 | 1.563 | 1.590 | 1.384 | 1.535 | 1.551 |

^aAbbreviations (see Figure 3): A: adsorbate; B: boron atom within the second diamond C layer; C1a, C1b, C1c: carbon atoms in the first diamond C layer, directly binding to the B atom; C2: carbon atom in the second diamond C layer; C3a: carbon atom in the third diamond C layer, directly binding to the B atom.

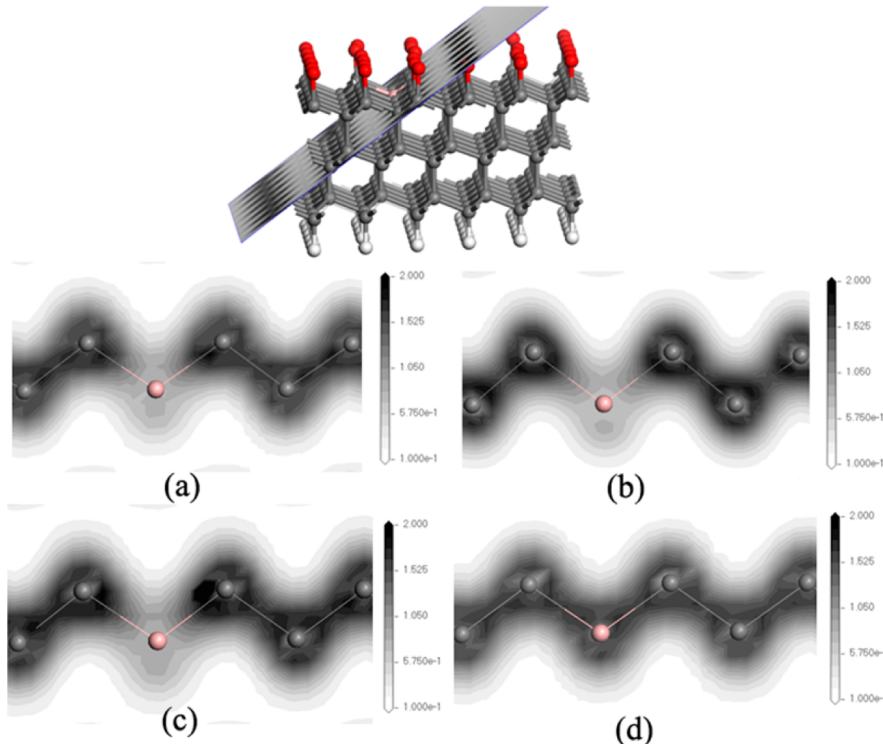


Figure 4. 2D slices showing the total electron density (ρ , in units of $e\text{\AA}^{-3}$) distribution maps for the B atom and its two binding surface C atoms for (a) H-terminated, (b) $\text{O}_{\text{on-top}}$ -terminated, (c) F-terminated, and (d) OH-terminated diamond (111) surfaces. The gray spheres are C atoms, and the pink ones are B atoms.

along the B–C bond (see Figure 4). As can be seen from the electron density maps in Figure 4a–d, the B–C bonds for the $\text{O}_{\text{on-top}}$ -terminated surfaces show the absolute least electronic density compared to the other three surface termination types (H, OH, and F). Furthermore, the adsorption $\text{O}_{\text{on-top}}$ was found to bind hardest to the surface in comparison with the other three termination types (shown in section 3.A). F- and H-terminated surfaces showed slightly less electron density along the B–C bond, as compared with neighboring C–C bonds. Furthermore, the situation is much more different for the OH-terminated surface. The electron density along the B–C bond is here found to be very similar to that for the surrounding C–C ones (see Figure 4b). This agrees well with the adsorption energy analyses in section 3.A where the OH-terminated surface showed the least effects of the adsorbates and surface C bond weakening in four terminated surfaces in the present study due to the steric repulsion. Also, H- and F-terminated surfaces showed a larger adsorption energy difference between $E_{\text{ads,avg}}$ and $E_{\text{ads,last}}$, which meant larger bond weakening induced by the B dopant.

All calculated electron bond populations, between the adjacent adsorbates (A) and the binding surface carbon atoms (C), are also shown in Table 3. The C–O bonds within the B-doped $\text{O}_{\text{on-top}}$ -terminated surface showed comparably large values of electron bond population (0.81–0.85) as compared with the nondoped scenario (0.77). This observation agrees very well with the bond length of the C–O bonds. Compared to the nondoped situation, the O-terminated surface showed a shortened C–A bond length.

On the other hand, the OH-terminated surface showed a somewhat smaller C–O bond population value for B doping (0.55), compared to nondoping (0.58). Moreover, the bonds

between the adjacent adsorbate and their binding surface C atom, for H- and F-terminated surfaces, showed almost identical bond population values when comparing B-doped with nondoped surfaces: H: 0.88 (B-doped) versus 0.89 (nondoped); and F: 0.44–0.45 (B-doped) versus 0.45 (nondoped). All results considering adsorbate–C_{surface} bond population values showed a good correlation with bond lengths (see section 3.B). This means that the bond population is inversely proportional to the bond length, that is, the longer the bond length, the smaller the bond population.

2. Electron Redistribution. The results obtained from the bond population analysis in section 3.C.1 were found to agree well with the conclusion that can be drawn from the Mulliken charges (as presented in Table 3). It can therefore be seen that the resulting atomic charge of B for the $\text{O}_{\text{on-top}}$ termination is +0.41 e, while the atomic B charges for the other three termination types are smaller, +0.39 (H), +0.36 (F), and +0.33(OH) e. As can furthermore be seen from Figure 4, for all B-doped diamond surfaces investigated, the surface carbon atoms gained electron density from the B atom, and thus, these atoms showed a more negative charge compared with C atoms farther away from the doped area. It also seems that the degree of electron transfer from the electropositive B dopant to the binding and more electronegative C atoms is most profound for the $\text{O}_{\text{on-top}}$ -terminated diamond surfaces.

To be more specific, for the H-terminated surfaces, the C–H bonds will be polarized with a negative charge on the C atom and a positive charge on the H atom. The origin of this dipole formation is the difference in electronegativity with a value of 2.20 for H and 2.55 for C.³⁷ The atomic charge of the surface C atom, being bonded to the B dopant (C1a), is −0.40, which is to be compared with the corresponding C atom (C1) in

Table 3. Results from the Atomic Charge Calculations (in e) for the Adsorbates, B Dopant, and Carbon Atoms Binding to the B Atom In Addition to Results from the Mulliken Bond Population Analysis for the B–C and A–C Bonds within the B-Doped Diamond (111) Surfaces with Different Adsorbates^a

| | | s | p | total | charge | bond type | bond population |
|---------------------|-------|------|------|-------|--------|-----------|-----------------|
| H | A1 | 0.80 | 0.00 | 0.80 | 0.20 | C1a–A1 | 0.88 |
| | A2 | 0.80 | 0.00 | 0.80 | 0.20 | C1b–A2 | 0.88 |
| | A3 | 0.80 | 0.00 | 0.80 | 0.20 | C1c–A3 | 0.88 |
| | A | 0.77 | 0.00 | 0.77 | 0.23 | C1–A | 0.89 |
| | B | 0.64 | 1.97 | 2.61 | 0.39 | | |
| | C1a | 1.22 | 3.18 | 4.40 | -0.40 | B–C1a | 0.80 |
| | C1b | 1.22 | 3.18 | 4.40 | -0.40 | B–C1b | 0.77 |
| | C1c | 1.22 | 3.17 | 4.39 | -0.39 | B–C1c | 0.82 |
| | C1 | 1.18 | 3.05 | 4.24 | -0.24 | C1–C2 | 0.81 |
| | C3a | 1.33 | 3.01 | 4.14 | -0.14 | B–C3a | 0.82 |
| | C3 | 1.10 | 2.90 | 4.00 | 0.00 | C2–C3 | 0.80 |
| | | | | | | | |
| O _{on-top} | A1 | 1.88 | 4.36 | 6.25 | -0.25 | C1a–A1 | 0.85 |
| | A2 | 1.89 | 4.34 | 6.23 | -0.23 | C1b–A2 | 0.84 |
| | A3 | 1.88 | 4.35 | 6.24 | -0.24 | C1c–A3 | 0.81 |
| | A | 1.89 | 4.39 | 6.28 | -0.28 | C1–A | 0.77 |
| | B | 0.71 | 1.87 | 2.59 | 0.41 | | |
| | C1a | 1.07 | 2.78 | 3.85 | 0.15 | B–C1a | 0.65 |
| | C1b | 1.08 | 2.79 | 3.87 | 0.13 | B–C1b | 0.67 |
| | C1c | 1.07 | 2.78 | 3.85 | 0.15 | B–C1c | 0.70 |
| | C1 | 1.04 | 2.69 | 3.73 | 0.27 | C1–C2 | 0.73 |
| | C3a | 1.12 | 3.03 | 4.15 | -0.15 | B–C3a | 0.86 |
| | C3 | 1.10 | 2.91 | 4.00 | 0.00 | C2–C3 | 0.82 |
| | | | | | | | |
| F | A1 | 1.94 | 5.36 | 7.32 | -0.32 | C1a–A1 | 0.44 |
| | A2 | 1.94 | 5.39 | 7.33 | -0.33 | C1b–A2 | 0.45 |
| | A3 | 1.94 | 5.36 | 7.30 | -0.30 | C1c–A3 | 0.44 |
| | A | 1.94 | 5.37 | 7.31 | -0.31 | C1–A | 0.45 |
| | B | 0.62 | 2.02 | 2.64 | 0.36 | | |
| | C1a | 1.10 | 2.71 | 3.81 | 0.19 | B–C1a | 0.80 |
| | C1b | 1.10 | 2.73 | 3.83 | 0.17 | B–C1b | 0.73 |
| | C1c | 1.10 | 2.70 | 3.81 | 0.19 | B–C1c | 0.82 |
| | C1 | 1.06 | 2.60 | 3.66 | 0.34 | C1–C2 | 0.80 |
| | C3a | 1.21 | 3.03 | 4.15 | -0.15 | B–C3a | 0.80 |
| | C3 | 1.10 | 2.90 | 4.00 | 0.00 | C2–C3 | 0.77 |
| | | | | | | | |
| OH | A(H)1 | 0.52 | 0.00 | 0.52 | 0.48 | | |
| | A(H)2 | 0.51 | 0.00 | 0.51 | 0.49 | | |
| | A(H)3 | 0.52 | 0.00 | 0.52 | 0.48 | | |
| | A(H) | 0.52 | 0.00 | 0.52 | 0.48 | | |
| | A(O)1 | 1.79 | 4.87 | 6.66 | -0.66 | C1a–A1 | 0.55 |
| | A(O)2 | 1.80 | 4.86 | 6.66 | -0.66 | C1b–A2 | 0.55 |
| | A(O)3 | 1.80 | 4.88 | 6.68 | -0.68 | C1c–A3 | 0.55 |
| | A(O) | 1.79 | 4.90 | 6.68 | -0.68 | C1–A | 0.58 |
| | B | 0.62 | 2.05 | 2.67 | 0.33 | | |
| | C1a | 1.11 | 2.82 | 3.94 | 0.06 | B–C1a | 0.82 |
| | C1b | 1.11 | 2.84 | 3.95 | 0.05 | B–C1b | 0.81 |
| | C1c | 1.11 | 2.83 | 3.94 | 0.06 | B–C1c | 0.84 |
| | C1 | 1.07 | 2.71 | 3.78 | 0.22 | C1–C2 | 0.81 |
| | C3a | 1.12 | 3.03 | 4.15 | -0.15 | B–C3a | 0.80 |
| | C3 | 1.10 | 2.91 | 4.00 | 0.00 | C2–C3 | 0.79 |
| | | | | | | | |
| clean | B | 0.64 | 2.01 | 2.64 | 0.36 | | |
| | C1a | 1.18 | 2.91 | 4.09 | -0.09 | B–C1a | 0.94 |
| | C1b | 1.18 | 2.92 | 4.10 | -0.10 | B–C1b | 0.94 |
| | C1c | 1.19 | 2.93 | 4.12 | -0.12 | B–C1c | 0.92 |
| | C1 | 1.13 | 2.82 | 3.95 | 0.05 | C1–C2 | 0.87 |
| | C3a | 1.16 | 2.84 | 4.00 | 0.00 | B–C3a | 0.39 |
| | C3 | 1.12 | 2.86 | 3.99 | 0.01 | C2–C3 | 0.64 |

^aThe abbreviations are the same as those used in Table 2.

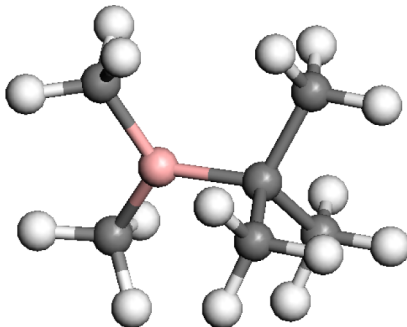


Figure 5. A model of the molecule $\text{H}_6\text{C}_2\text{BC}_3\text{H}_9$. The bond population of the B–C bond is 0.87, and the corresponding bond length is 1.596 Å.

nondoped diamond (111), –0.24. This is expected because the electronegativity for B is smaller than that for C. For the terminating species that are more electronegative than the element C, the atomic charges of C1a versus C1 will be positive. For the terminating species $\text{O}_{\text{on-top}}$, F, and OH, the atomic charges are +0.15 (+0.27), +0.19 (+0.34), and +0.06 (+0.22), respectively. For each couple of values, the first value represents the doping situation (C1a), and the value within parentheses represents the nondoping situation (C1). It is hence completely clear that there is a withdrawal of electrons from the B element to these types of electronegative adsorbates.

These results are further emphasized when calculating the charges of the adjacent adsorbates, which were furthermore observed to undergo slight changes when substituting C with B in the lattice. For both the B-doped and nondoped situation, the partial electron transfer between the terminating species and the binding surface C atoms followed the differences in electronegativity. The calculated atomic charges for $\text{O}_{\text{on-top}}$ (–0.24 for doping versus –0.28 for nondoping), OH (atomic charge for the oxygen: –0.55 for doping versus –0.58 for nondoping), F (–0.32 for doping versus –0.31 for doping) all indicated partial electron transfer from the surface C to the respective adsorbate. For the situation with H-termination (i.e., with a less electronegative value compared to C), the opposite situation was observed (+0.20 for doping versus +0.23 for nondoping). This result is understandable because the electron density at C1a is higher than that at C1 due to the presence of B with its tendency to withdraw electrons toward its surrounding C atoms (thereby lowering the withdrawal capability of C1a with respect to the terminating H). It is interesting to note that a smaller electron density is moved from the adsorbate H to the binding surface C atoms, while it should have been the opposite if the results were completely based on the differences in electronegativity. Again, this is a clear effect of B doping. In addition, the degree of electron transfer toward the $\text{O}_{\text{on-top}}$ adsorbates, for the B doping situation, was smaller than the corresponding transfer for a nondoped situation ($\text{O}_{\text{on-top}}$ charge of –0.24 versus –0.28). The situation is identical for the OH adsorbates (O (in OH) charge of –0.67 versus –0.68). However, the situation was different for F termination, where the effect of B doping on the electron distribution is not completely clear due to larger variation in F atomic charges. However, by looking at the averaged atomic charges for the three adjacent F adsorbates (–0.32 versus –0.31), the B dopant effect will be similar to the H termination situation in the way that the degree of electron

transfer will increase by introducing B dopants into the diamond lattice, either toward F (making F more negative) or from H (making H more positive).

3. Spin Density. The spin density maps for all systems under investigations are plotted in Figure 6. These maps show the difference between α - and β -electron densities (i.e., spin up versus spin down). If the α -spin density is dominating over the corresponding β -spin values, a positive value will be the result in these plots. In a similar manner, an excess of β -spin densities will give a negative value. These spin density maps make it possible to visualize the resulting spin distribution for the various systems and especially to get some information about the combined effect of B doping and surface termination. For all types of surface termination that was used in the present study, the electron spin density was observed to surround the bonds between the B dopant and the surface C atoms (see Figure 6). The H-, OH-, and F-terminated surfaces looked very similar in that the α -spin is dominating. It is thereby possible to draw the conclusion that the deficiency of electrons in the B dopant showed a rather local impact on the B–C bonds and in this case for only two of total of three bonds. In addition, the F-terminated surface showed a numerically larger value of the spin density ($0.16/\text{\AA}^3$) compared with the H- and OH-terminated surfaces (0.08 versus and $(0\text{--}0.10/\text{\AA}^3)$ (see Figure 6a,c,d). It is worth noticing that the two spin-polarized B–C bonds in the H-, OH-, and F- terminated surfaces will also display longer bond lengths (Table 2) and smaller bond population values (Table 3) compared to the other two B–C bonds surrounding B in the diamond lattice. The observation is, thereby, that the weaker the B–C bond (with longer bond length and less electron density), the larger the spin density along the bond. It is thereby possible to draw the conclusion that the bonding state of the B–C bond is no longer completely filled by electrons. In addition to the localized B–C bond spin densities, a minor spin density was also found to distribute at the three adjacent F adsorbates (Aa, Ab, Ac) for the F-terminated surface and at some OH adsorbates for the OH-terminated surface. This observation is most probably caused by the large values of electronegativity of the F and OH adsorbates. This result is clearly supported by the observation made in section 3.C.2, which clearly shows that electrons from the B dopant will be attracted to adjacent F and OH adsorbates.

It is also here obvious that O in the on-top position will induce a special effect on the diamond surface and its properties. The $\text{O}_{\text{on-top}}$ adsorbate shows a large spin density, and the isosurface visualizes a mixture of both α - and β -spins that are distributed over the diamond surface and located at the various $\text{O}_{\text{on-top}}$ adsorbates. This is an observation that is completely different from the other termination situations. The underlying reason for these high spin density values ($0.06/\text{\AA}^3$) is the radical nature of the O adsorbate. The bond population analysis shows that the numerical value of the bond order for this type of C–O bond is around 0.8. It is hence close to a C–O single bond instead of the C=O double bond. Because the O element has six valence electrons, a monoradical O adsorbate must be formed when attached to the diamond surface with only one covalent bond (Figure 6b). The fact that both spin-up and spin-down types of spin densities are present among the $\text{O}_{\text{on-top}}$ adsorbates is most probably due to spatial repulsions. This distribution of spins for the $\text{O}_{\text{on-top}}$ termination is clearly visible in Figure 6d.

4. Fukui Functions (FFs). A FF is the differential change in electron density when an infinitesimal number of electrons is

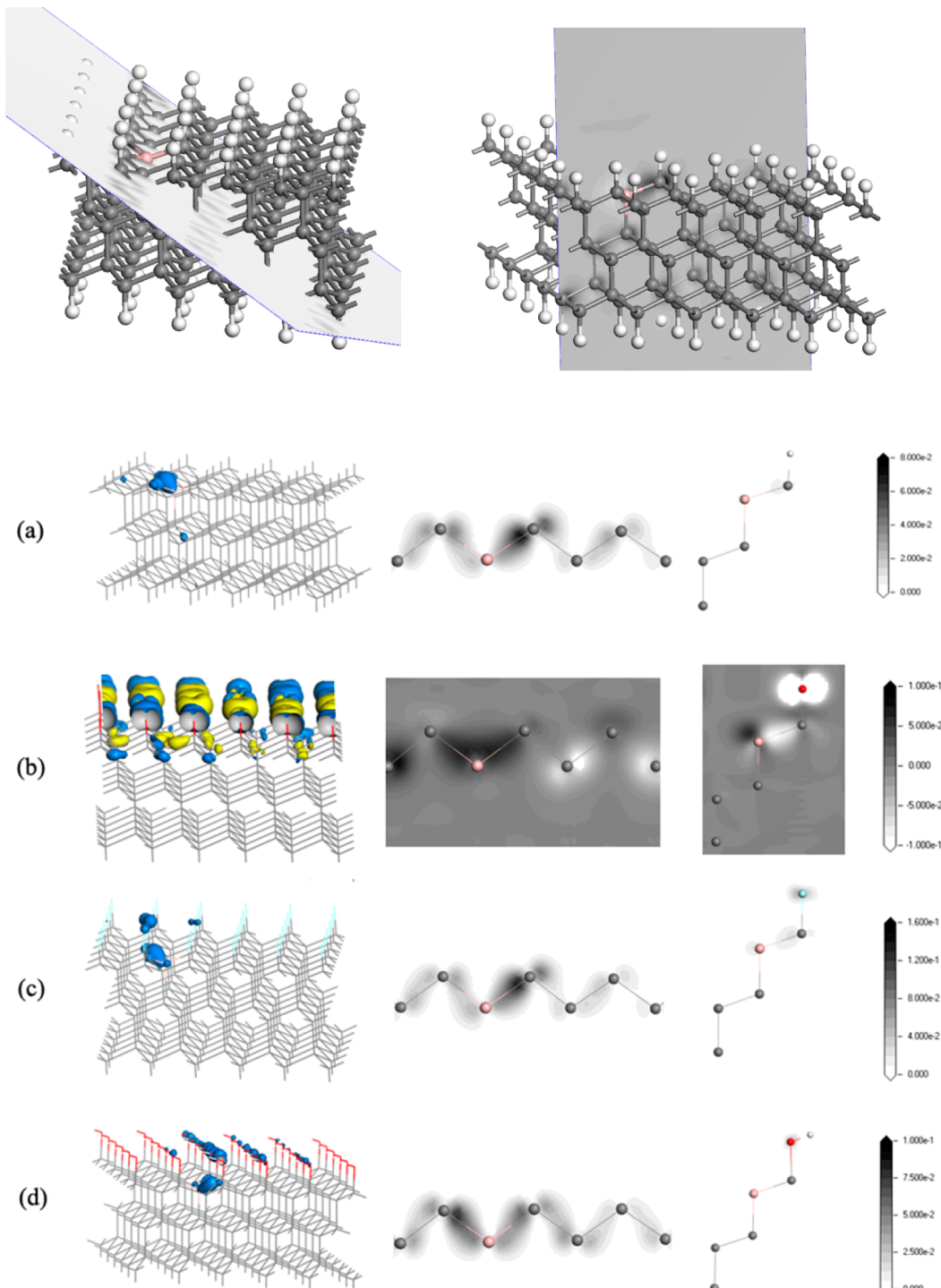


Figure 6. Spin density maps for the supercell models of B-doped diamond (111) surfaces with (a) H termination (isosurface = $0.025/\text{\AA}^3$), (b) $\text{O}_{\text{on-top}}$ termination (isosurface = $0.04/\text{\AA}^3$), (c) F termination (isosurface = $0.05/\text{\AA}^3$), and (d) OH termination (isosurface = $0.06/\text{\AA}^3$) (left column). The 2D slices of spin density C–B–C planes (middle column) and spin density C–B–A planes (right column) are shown on the right-hand side of this figure. The dark-colored spheres show the C atoms and the bright-colored ones the B atoms. The 3D spin density is shown on the left-hand side of the figure. It is only the $\text{O}_{\text{on-top}}$ -terminated surface (d) that shows an isosurface with both positive (dark color) and negative values (bright color).

either added to or removed from the system under investigation.³⁰ It has here been used as a quite helpful tool to predict the distribution of chemical reactivity on the surface from intrinsic electronic properties. As presented in section 3.C.2, the FFs will give qualitative information with respect to electrophilic, nucleophilic, and radical attack of the various surface sites. As presented in Figure 7, the maps of 2D FFs are

colored from white (which visualizes the smallest value and is hence least susceptible to the specific attack) to black (which represents the largest value and shows the most susceptible surface sites with respect to the specific attack). As can be seen in Figure 7, the FFs are largest for the three adjacent adsorbates to the B dopant and are hence the most reactive ones. However, the degree of reactivity differs a lot between the

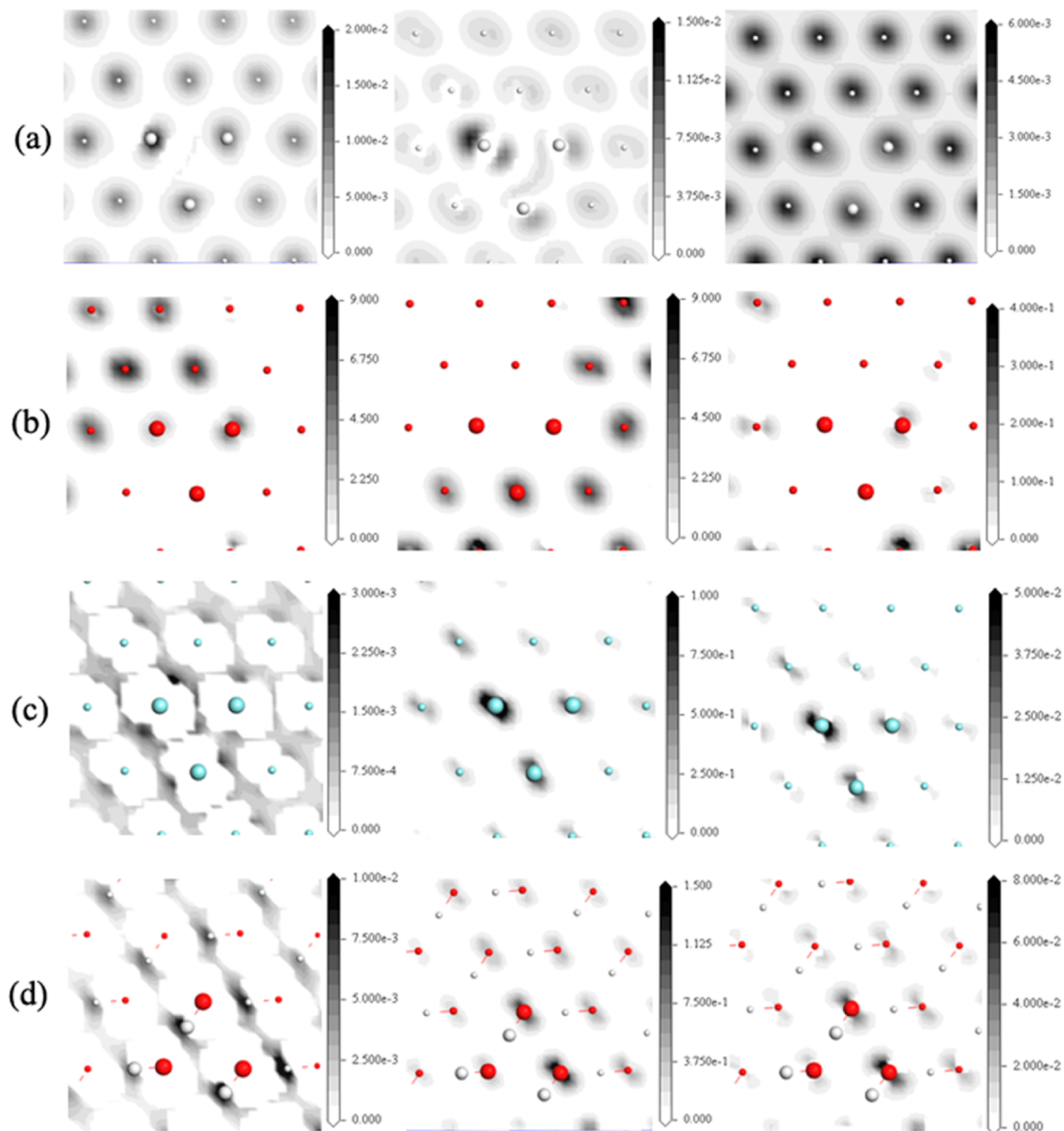


Figure 7. FFs mapped onto the 2D isosurface charge density of the adsorbates [(a) H, (b) O_{on-top}, (c) F, or (d) OH] attached to diamond (111), showing the susceptibility of electrophilic (left column), nucleophilic (middle column), and radical (right column) attack. The bigger spheres in the slices represent the three adjacent adsorbates (linked to the surface C atoms that bind to the B dopant).

different adsorbate types, which in practice means that the susceptibility to a specific attack depends completely on the combined effect of B doping and surface termination. In the present section, only the most susceptible and reactive surface sites will be the target for discussions and comparisons.

The 100% H-terminated surfaces showed overall much smaller values of the FFs, even though the adjacent H atoms to the B dopant showed a somewhat larger tendency for reactivity (0.02 for electrophilic, 0.015 for nucleophilic, and 0.006 for radical). For the OH-terminated surface, the O atoms in two of these adsorbates were found to display a larger susceptibility (1.5) for a nucleophilic attack and a very minor susceptible (0.08) for a radical attack. On the other hand, the H atoms in

these OH adsorbates showed susceptibility toward electrophilic attack (0.02). The F-terminated adsorbates closest to the B dopant (especially one of them) showed large values (1) of susceptibility for a nucleophilic attack and a very minor susceptible (0.05) for a radical attack. In summary, for H-, OH-, and F-terminated surfaces, the FFs indicate that the B dopant will increase the reactivity for the adjacent C adsorbates to the B dopant. More specifically, the B dopant will largely induce susceptibility for a nucleophilic attack to (i) adjacent F adsorbates and to (ii) the O atoms in adjacent OH adsorbates.

The O_{on-top}-terminated surface is also in this sense completely different from the other terminated surfaces. First of all, we have here the largest susceptibility toward an attack

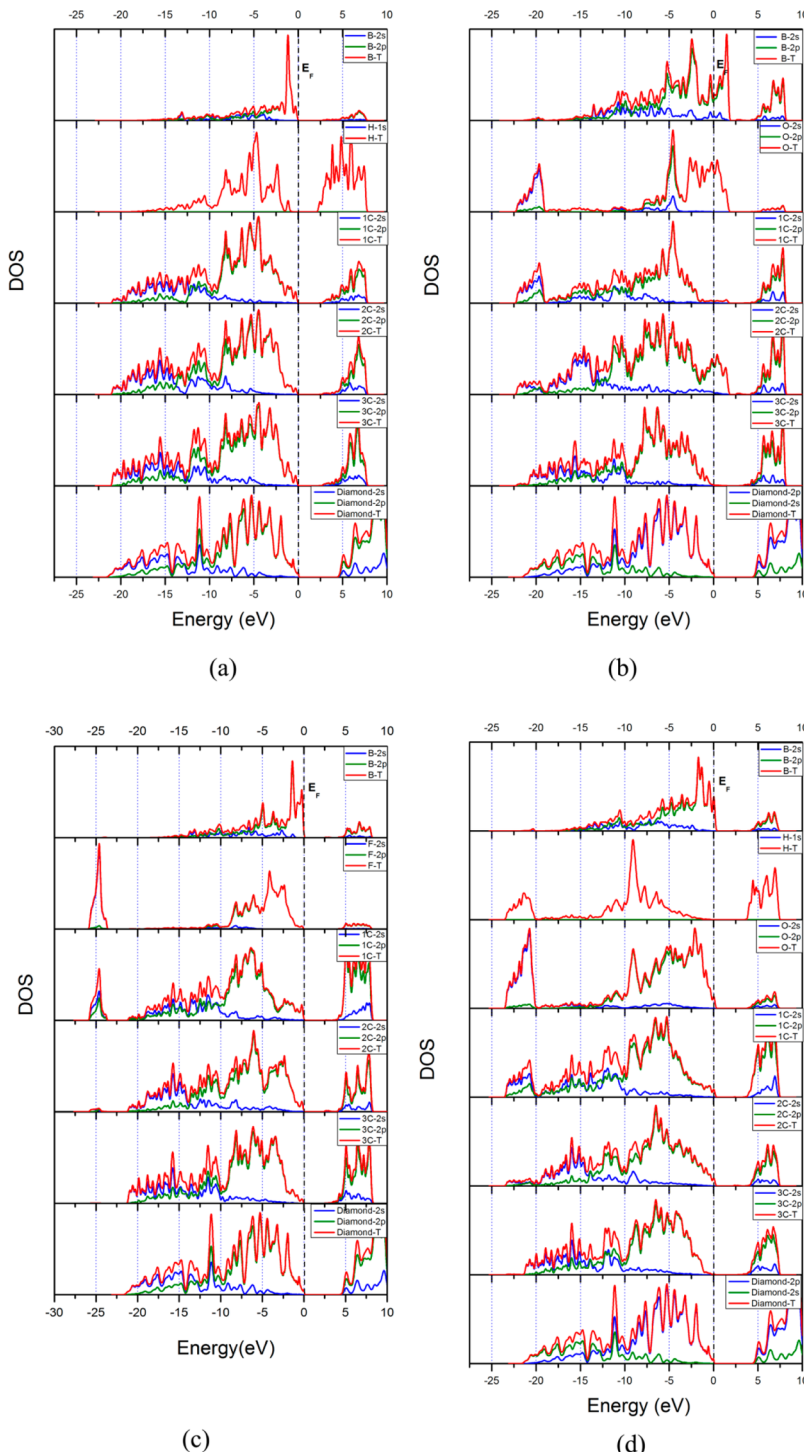


Figure 8. The pDOS for the diamond (111) surface with (a) H termination, (b) O_{on-top} termination, (c) F termination, and (d) OH termination. For each terminating species, the various pDOS spectra show (from top to down) pDOS for the specific adsorbate, the top three C layers (1C, 2C, 3C), the B dopant, and bulk (nondoped) diamond. Blue line: pDOS (s orbitals); green line: pDOS (p orbitals); red line: DOS (total).

from, for example, gaseous species. Half of the O_{on-top} adsorbates show a strong susceptibility toward an electrophilic attack, and the remaining half of the O_{on-top} adsorbates show a strong susceptibility to a nucleophilic attack (with a value of 9 for each). This is reasonable because the radical O adsorbates, with their one unpaired electron, must be very reactive and thus will react strongly with both electrophilic and nucleophilic species. What is also interesting for this type of termination type is that the adjacent O adsorbates even showed less

susceptibility for attacks compared to O adsorbates farther away from the B doping site. This agrees very well with the Mulliken population analysis described in section 3.C.2 because the adjacent O_{on-top} species showed less negative atomic charges (due to the effect of the B dopant) and therefore would be less reactive than other O_{on-top} adsorbates.

D. Total and Partial Densities of States. Figure 8 shows the partial density of states (pDOS) for the B-doped diamond (111) surfaces with four different types of terminating species.

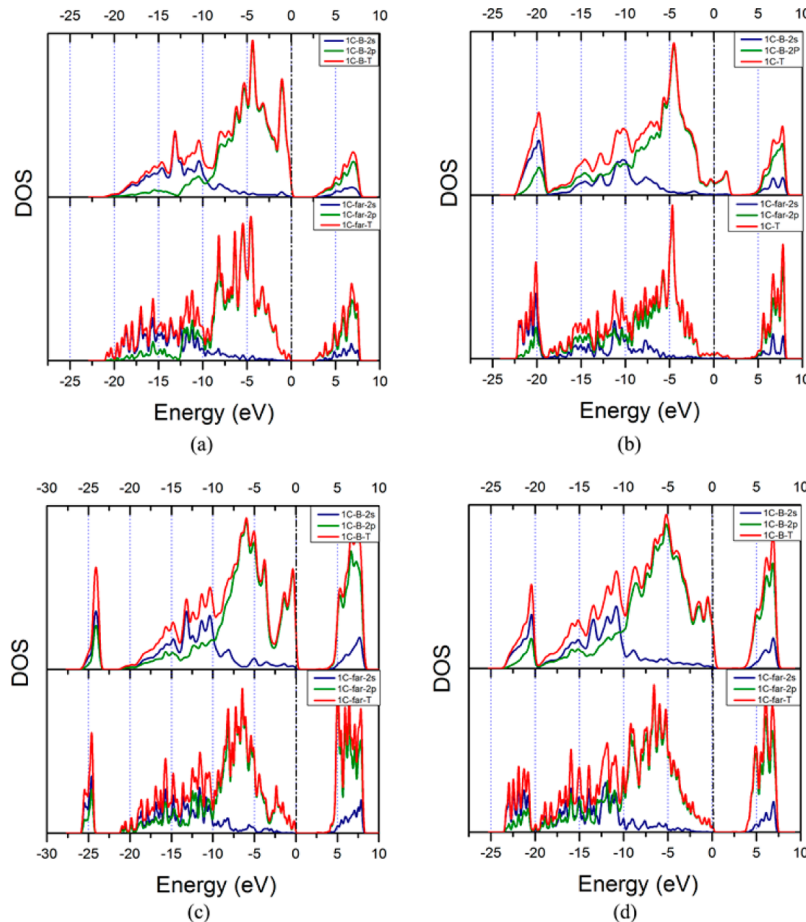


Figure 9. pDOS for the diamond (111) surface with (a) H termination, (b) O_{on-top} termination, (c) F termination, and (d) OH termination. The pDOS of three surface carbon atoms bonded to the B dopant (named 1C–B) and one surface carbon atom far away from B dopant (named 1C-far) from the top down each graph. Blue line: pDOS (s orbitals); green line: pDOS (p orbitals); red line: DOS (total).

For comparison, the complete DOS of nondoped bulk diamond is also shown at the bottom of each figures. It is a well-known fact that the band gap will be underestimated when using DFT calculations, and the present method shows that the calculated band gap for bulk diamond is 4.8 eV (see Figure 8), which is compared to the experimental value of 5.5 eV.³⁸ In order to study the detailed information regarding the effect of B dopant and adsorbates, the pDOSs for the different atomic layers (from adsorbates down to the third-layer C atoms) are shown in Figure 8.

For the H-terminated surface, there are no observable differences between the pDOSs of the different C atomic layers in the system (excluding the B dopant). Earlier studies have shown that H-terminated diamond surfaces under atmospheric conditions will induce p-type surface doping.^{39,40} As can be seen in Figure 8a, the estimated band gaps for the upper three carbon layers are 2.5 eV, which is quite smaller than the value for bulk diamond. The smaller band gap for the surface carbons is most probably affected predominantly by the terminating H atoms. For detailed observation of the B dopant effect, the pDOS of three surface C atoms that bonded to the B dopant (1C–B) is plotted in Figure 9a, compared to the pDOS of the surface C atom far away from doping area (1C-far). A small electron hole above the Fermi level appears in the pDOS of 1C–B, which is clearly characteristic of a p-type doping material.⁴¹ The peak within the range of −0.5 to −1.5 eV shown in 1C–B is a characteristic peak of the B dopant that

cannot be found in 1C-far. It indicated that the effects of the B dopant can be quite local and not extend to a large area.

The pDOSs for the O_{on-top}-terminated diamond surface are presented in Figure 8b. The pDOSs of the O atoms extend above the Fermi level (within an energy range of 2 eV). These states are most probably induced by the unpaired 2p electrons on the radical O atoms. More generally, the 2p electrons at these O adsorbates show a concentration of DOS in the vicinity of the Fermi level. Thus, the O_{on-top}-terminated diamond (111) surface is quite reactive and also electronically conductive, which agrees with earlier observations made by Derry et al.⁴² These authors have also predicted that O-terminated diamond (111) surfaces are metallic (or conducting) due to the fact that the Fermi level is positioned within the occupied upper-level DOS.

The O_{on-top}-terminated surface is also quite exceptional compared to the other termination scenarios, in that both the B dopant and the surrounding C atoms in the second layer significantly contribute to the surface electronic conductivity. There are some occupied 2p electron states above the Fermi level that originate from terminated O atoms. The characteristic pDOS peaks of adsorbed O in on-top positions are located within the ranges of −19 to −22 and −4 to −5 eV. Similar positions of peaks for first-layer and second-layer C atoms exist but with decreasing intensity. This is a fingerprint of the fact that there is a strong interaction between the O adsorbates and the binding surface C atoms. As can be seen in Figure 8, the

interactions between the O adsorbates and the third atomic layer C atoms have diminished to 0. However, what is most interesting here are the pDOS peaks in the interval of 0–2.2 eV (resulting from especially the radical O adsorbate, B dopant, and C in layer 2 and with a minor contribution from C atoms in layer 1), indicating a very strong interaction between these atoms.

Figure 8c shows the pDOSs of B-doped diamond (111) surfaces that are F-terminated. As was the situation with O_{on-top} termination, there is a clear overlap between O 2p electron peaks within the interval of –26 to –24 eV and especially the binding C atom in the first atomic C layer (being a strong indication of surface C–F binding). Unlike H termination, the band gap did not seem to change for the upper diamond (111) surface (as compared with nondoped bulk diamond).

The pDOS spectra for an OH-terminated B-doped diamond surface showed an almost identical feature as the F-terminated ones. Overlapping peaks (–23.5 to –20 eV), involving OH and the first-layer C atoms, indicated strong adsorbate–surface interactions, which declined rapidly down into the C lattice. In addition, the band gap, as compared to that for nondoped bulk diamond, did not seem to change much for the upper diamond (111) surface. As was the situation with H termination, one small hole appeared above the Fermi level in the pDOSs of the F- and OH-terminated surfaces, as presented in Figures 9c,d, respectively. The characteristic peak of the B dopant appears below the Fermi level also in the pDOS of 1C–B, which cannot be found in the pDOS of 1C-far. This again proves the local effect induced by the B dopant.

4. CONCLUSION AND SUMMARY

From these results, it is possible to conclude that for both nondoped and B-doped diamond (111) surface scenarios, the trend in the averaged adsorption energy (as a function of surface terminating species) is OH < H < F < O_{on-top}. The adsorption energies were also found to be numerically quite similar for the adsorbates H, OH, and F. The B dopant, substitutionally positioned within the diamond (111) surface, was found to have a very minor influence on the averaged adsorption energy for the various terminating species investigated. However, the B dopant can have an obvious influence on the adjacent adsorbates. It was here found to destabilize the adjacent surface–adsorbate bonds, with the following trend for the various surface termination species, OH < O_{on-top} < H < F.

The electronic structure results agreed with the geometrical structure analysis. The considerable change of atomic charges takes place in the four carbon atoms bonded to the B dopant. In addition, the B dopant was found to increase the reactivity of adjacent H, OH, and F adsorbates and decrease the reactivity of adjacent O adsorbates.

Finally, comparing the four DOSs of the B atoms in the diamond surfaces with four different species, the shapes of the valence and conduction bands in the DOS are quite different, which is largely affected by the adsorbed terminated species. The B dopant may have a local influence on the pDOS of B-bonded surface carbon atoms and not extend to a large area. The influence induced by the terminated species can only affect the DOS of the first two surface carbon layers, but the third layer displays very little influence by the adsorbates and is already close to the bulk diamond DOS.

AUTHOR INFORMATION

Notes

The authors declare no competing financial interest.

ACKNOWLEDGMENTS

This work was supported by the Swedish Research Council (VR). The computational results were obtained using CASTEP from Accelrys.

REFERENCES

- (1) McCreery, R. Advanced Carbon Electrode Materials for Molecular Electrochemistry. *Chem. Rev.* **2008**, *108*, 2646–2687.
- (2) Panizza, M.; Cerisola, G. Application of Diamond Electrodes to Electrochemical Processes. *Electrochim. Acta* **2005**, *51*, 191–199.
- (3) Luong, J.; Male, K.; Glennon, J. Boron-Doped Diamond Electrode: Synthesis, Characterization, Functionalization and Analytical Applications. *Analyst* **2009**, *134*, 1965–1979.
- (4) Sabine, S.; Yannick, C.; Elisabeth, G.; Josef, B.; Rabah, B. Preparation of Boron-Doped Diamond Nanowires and Their Application for Sensitive Electrochemical Detection of Tryptophan. *Electrochim. Commun.* **2010**, *12*, 438–441.
- (5) Marcon, L.; Spriet, C.; Coffinier, Y.; Galopin, E.; Rosnoble, C.; Szunerits, S.; Héliot, L.; Andrand, P.-O.; Boukherroub, R. Cell Adhesion Properties on Chemically Micropatterned Boron-Doped Diamond Surfaces. *Langmuir* **2010**, *26*, 15065–15069.
- (6) Celii, F.; Butler, J. Hydrogen Atom Detection in the Filament-Assisted Diamond Deposition Environment. *Appl. Phys. Lett.* **1989**, *54*, 1031–1033.
- (7) Denisenko, A.; Romanyuk, A.; Kibler, L. A.; Kohn, E. Surface Structure and Electrochemical Characteristics of Boron-Doped Diamond Exposed to rf N₂-Plasma. *J. Electroanal. Chem.* **2011**, *657*, 164–171.
- (8) Szunerits, S.; Boukherroub, R. Different Strategies for Functionalization of Diamond Surfaces. *J. Solid State Electrochem.* **2008**, *12*, 1205–1218.
- (9) May, P. W.; Stone, J. C.; Ashfold, M. N. R.; Hallam, K. R.; Wang, W. N.; Fox, N. A. The Effect of Diamond Surface Termination Species upon Field Emission Properties. *Diamond Relat. Mater.* **1998**, *7*, 671–676.
- (10) Takeshi, K.; Hiroyuki, I.; Kazuhide, K.; Kazuhiro, O.; Yasuaki, E.; Akira, F.; Takeshi, K. Plasma Etching Treatment for Surface Modification of Boron-Doped Diamond Electrodes. *Electrochim. Acta* **2007**, *52*, 3841–3848.
- (11) Mackey, B. L.; Russell, J. N., Jr.; Crowell, J. E.; Butler, J. E. Effect of Surface Termination on the Electrical Conductivity and Broad-Band Internal Infrared Reflectance of a Diamond (110) surface. *Phys. Rev. B* **1995**, *52*, R17009–R17012.
- (12) René, H.; Armin, K.; Harald, O.; Jakob, H.; Marco, W.; Waldemar, S.; Nianjun, Y.; Christoph, E. N. Electrochemical Hydrogen Termination of Boron-Doped Diamond. *Appl. Phys. Lett.* **2010**, *97*, 052103/1–052103/3.
- (13) Garrido, J.; Härtl, A.; Dankerl, M.; Reitinger, A.; Eickhoff, M.; Helwig, A.; Müller, G.; Stutzmann, M. The Surface Conductivity at the Diamond/Aqueous Electrolyte Interface. *J. Am. Chem. Soc.* **2008**, *130*, 4177–4181.
- (14) De Theije, F.; Roy, O.; van Der Laag, N.; Van Enckevort, W. Oxidative Etching of Diamond. *Diamond Relat. Mater.* **2000**, *9*, 929–934.
- (15) Hutton, L.; Iacobini, J.; Bitziou, E.; Channon, R.; Newton, M.; Macpherson, J. Examination of the Factors Affecting the Electrochemical Performance of Oxygen-Terminated Polycrystalline Boron-Doped Diamond Electrodes. *Anal. Chem.* **2013**, *85*, 7230–7240.
- (16) Mei, W.; Nathalie, S.; Claudia, D.-P.; Muriel, B.; Arnaud, E.; Musen, L.; Rabah, B.; Sabine, S. Comparison of the Chemical Composition of Boron-Doped Diamond Surfaces upon Different Oxidation Processes. *Electrochim. Acta* **2009**, *54*, 5818–5824.

- (17) Ferro, S.; De Battisti, A. The 5-V Window of Polarizability of Fluorinated Diamond Electrodes in Aqueous Solutions. *Anal. Chem.* **2003**, *75*, 7040–7042.
- (18) Petrini, D.; Larsson, K. A Theoretical Study of the Energetic Stability and Geometry of Hydrogen- and Oxygen-Terminated Diamond (100) Surfaces. *J. Phys. Chem. C* **2007**, *111*, 795–801.
- (19) Petrini, D.; Larsson, K. Origin of the Reactivity on the Nonterminated (100), (110), and (111) Diamond Surfaces: An Electronic Structure DFT Study. *J. Phys. Chem. C* **2008**, *112*, 14367–14376.
- (20) Petrini, D.; Larsson, K. Theoretical Study of the Thermodynamic and Kinetic Aspects of Terminated (111) Diamond Surfaces. *J. Phys. Chem. C* **2008**, *112*, 3018–3026.
- (21) Kohn, W.; Sham, L. J. Self-Consistent Equations Including Exchange and Correlation Effects. *Phys. Rev.* **1965**, *140*, A1133–A1138.
- (22) Hohenberg, P.; Kohn, W. Inhomogeneous Electron Gas. *Phys. Rev.* **1964**, *136*, B864–B871.
- (23) Vanderbilt, D. Soft Self-Consistent Pseudopotentials in a Generalized Eigenvalue Formalism. *Phys. Rev. B* **1990**, *41*, 7892–7895.
- (24) Perdew, J. P.; Burke, K.; Ernzerhof, M. Generalized Gradient Approximation Made Simple. *Phys. Rev. Lett.* **1996**, *77*, 3865–3868.
- (25) Clark, S. J.; Segall, M. D.; Pickard, C. J.; Hasnip, P. J.; Probert, M. I. J.; Refson, K.; Payne, M. C. First Principles Methods Using CASTEP. *Z. Kristallogr.* **2005**, *220*, 567–570.
- (26) Monkhorst, H. J.; Pack, J. D. Special Points for Brillouin-Zone Integrations. *Phys. Rev. B* **1976**, *13*, 5188–5192.
- (27) Larsson, K. Surface Properties of Diamond under Atmospheric Conditions: A Quantum Mechanical Approach. *New Diamond Front. Carbon Technol.* **2005**, *15*, 229–245.
- (28) Segall, M. D.; Shah, R.; Pickard, C. J.; Payne, M. C. Population Analysis of Plane-Wave Electronic Structure Calculations of Bulk Materials. *Phys. Rev. B* **1996**, *54*, 16317–16320.
- (29) Yang, W.; Parr, R. G.; Pucci, R. Electron-Density, Kohn–Sham Frontier Orbitals, and Fukui Functions. *J. Chem. Phys.* **1984**, *81*, 2862–2863.
- (30) Parr, R. G.; Yang, W. T. Density Functional-Approach to the Frontier-Electron Theory of Chemical-Reactivity. *J. Am. Chem. Soc.* **1984**, *106*, 4049–4050.
- (31) Fukui, K. Role of Frontier Orbitals in Chemical-Reactions. *Science* **1982**, *218*, 747–754.
- (32) Fukui, K.; Yonezawa, T.; Shingu, H. A Molecular Orbital Theory of Reactivity in Aromatic Hydrocarbons. *J. Chem. Phys.* **1952**, *20*, 722–725.
- (33) Delley, B. An All-Electron Numerical-Method for Solving the Local Density Functional for Polyatomic-Molecules. *J. Chem. Phys.* **1990**, *92*, 508–517.
- (34) Delley, B. From Molecules to Solids with the DMol(3) Approach. *J. Chem. Phys.* **2000**, *113*, 7756–7764.
- (35) Pfrommer, B. G.; Côté, M.; Louie, S. G.; Cohen, M. L. Relaxation of Crystals with the Quasi-Newton Method. *J. Comput. Phys.* **1997**, *131*, 233–240.
- (36) Ying-Gang, L.; Stuart, T.; Johan, V.; Stoffel, D. J.; Ken, H.; Gustaaf Van, T. Local Bond Length Variations in Boron-Doped Nanocrystalline Diamond Measured by Spatially Resolved Electron Energy-Loss Spectroscopy. *Appl. Phys. Lett.* **2013**, *103*, 032105.
- (37) Allred, A. L. Electronegativity Values from Thermochemical Data. *J. Inorg. Nucl. Chem.* **1961**, *17*, 215–221.
- (38) Yokoya, T.; Nakamura, T.; Matsushita, T.; Muro, T.; Takano, Y.; Nagao, M.; Takenouchi, T.; Kawarada, H.; Oguchi, T. Origin of the Metallic Properties of Heavily Boron-Doped Superconducting Diamond. *Nature* **2005**, *438*, 647–650.
- (39) Ristein, J.; Riedel, M.; Maier, F.; Mantel, B. F.; Stammler, M.; Ley, L. Surface Doping: A Special Feature of Diamond. *J. Phys.: Condens. Matter* **2001**, *13*, 8979.
- (40) Petrini, D.; Larsson, K. Electron-Transfer Doping on a (001) Surface of Diamond: Quantum Mechanical Study. *J. Phys. Chem. B* **2005**, *109*, 22426–22431.
- (41) Yamamoto, T.; Katayama-Yoshida, H. Solution Using a Codoping Method to Unipolarity for the Fabrication of p-Type ZnO. *Jpn. J. Appl. Phys.* **1999**, *38*, L166–L169.
- (42) Derry, T.; Makau, N.; Stampfl, C. Oxygen Adsorption on the (1 × 1) and (2 × 1) Reconstructed C(111) Surfaces: A Density Functional Theory Study. *J. Phys.: Condens. Matter* **2010**, *22*, 265007.